Inorganic Chemistry

Article

pubs.acs.org/IC

Structure Refinement and Two-Center Luminescence of $Ca_3La_3(BO_3)_5:Ce^{3+}$ under VUV−UV Excitation

Chunmeng Liu,[†] Hongbin Liang,*[,†] Xiaojun Kuang,[†] Jiuping Zhong,[†] Shuaishuai Sun,[‡] and Ye Tao[‡]

[†]MOE Laboratory of Bioinorganic and Synthetic Chemistry, KLGHEI of Environment and Energy Chemistry, State Key Laboratory of Optoelectronic Materials and Technologies, School of Chemistry and Chemical Engineering, Sun Yat-sen University, Guangzhou 510275, China

[‡]Beijing Synchrotron Radiation Facility, Institute of High Energy Physics, Chinese Academy of Sciences, Beijing 100039, China

Supporting Information

ABSTRACT: A series of $Ca_3La_{3(1-x)}Ce_{3x}(BO_3)_5$ phosphors were prepared by a high-temperature solid-state reaction technique. Rietveld refinement was performed using the powder X-ray diffraction (XRD) data, which shows occupation of Ce^{3+} on both Ca^{2+} and La^{3+} sites with a preferred location on the La^{3+} site over the Ca^{2+} site. The prepared samples contain minor second phase $LaBO_3$ with contents of ∼0.64−3.27 wt % from the Rietveld analysis. $LaBO_3$:1%Ce^{3+} was prepared as a single phase material and its excitation and emission bands were determined for identifying the influence of impurity $LaBO_3:Ce^{3+}$ luminescence on the spectra of the $Ca_3La_{3(1-x)}Ce_{3x}(BO_3)_5$ samples. The luminescence properties of $Ca_3La_{3(1-x)}Ce_{3x}(BO_3)_5$ samples under vacuum ultraviolet (VUV) and UV excitation were investigated, which exhibited two-center luminescence of Ce^{3+}, assigned to the $Ce(1)^{3+}$ center in the La^{3+} site and $Ce(2)^{3+}$ center in the Ca^{2+} site, taking into account the spectroscopic properties and the Rietveld refinement results. The influences of the doping concentration and the excitation wavelength on the luminescence of Ce^{3+} in $Ca_3La_{3(1-x)}Ce_{3x}(BO_3)_5$ are discussed together with the decay characteristics.

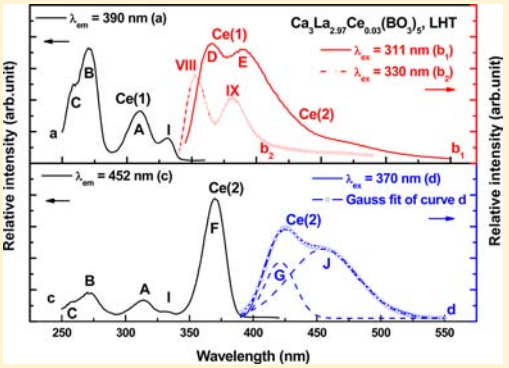

1. INTRODUCTION

Luminescence of Ce^{3+} in complex oxides has been developed for applications in lightings,[1−3] displays,[4] and medical imaging detectors.[5] For these applications, Ce^{3+} ions are either activators or sensitizers.[6] Moreover, the knowledge on the 4f−5d transitions of Ce^{3+} in a specific host lattice makes it possible to estimate the locations of the energy levels for other lanthanide ions in the same site of a certain host.[7] The luminescence of Ce^{3+} is also useful for identifying the number of lattice sites occupied by Ce^{3+} in a specific host.[8] The site occupancy for Ce^{3+} in a host may be considered as a reference for other lanthanide ions in the same host lattice, because trivalent lanthanide ions have similar ionic radii. So the investigation on the spectroscopic properties of Ce^{3+} in different host lattices is important not only for application but also for fundamental research.

Many lanthanides show efficient luminescence in borate compounds, and the luminescence properties of lanthanides in borates, such as $GdMgB_5O_{10}:Ce^{3+},Tb^{3+}$, $CaMgB_2O_5:Tb^{3+}$, and $(Y,Gd)BO_3:Eu^{3+}$, have been extensively studied and have gotten actual applications.[9] Recently $Ca_3La_3(BO_3)_5$ received attention as the host compound for luminescence. Han and co-workers obtained an efficient green VUV phosphor on Tb^{3+}-activated $Ca_3La_3(BO_3)_5$ with a short decay time.[10] Zhang et al. reported the red emission under UV excitation of Eu^{3+} in $Ca_3La_3(BO_3)_5$ from a sol−gel process.[11] The structure of $Ca_3La_3(BO_3)_5$ was first solved by Zhang[12] from the powder XRD data and then confirmed by Zhou[13] using the single-crystal X-ray diffraction data. The structure consists of isolated triangle BO_3 groups with large cations La^{3+} and Ca^{2+} located in 10-coordinate and 8-coordinate environments, respectively, which are able to accommodate the lanthanide elements and thus may serve as a host for two-center luminescence.

Here we report the structure and luminescence of $Ca_3La_{3(1-x)}Ce_{3x}(BO_3)_5$ phosphors. The materials exhibit two-center luminescence, consistent with the occupation of Ce^{3+} on both the La^{3+} and Ca^{2+} sites, as revealed by the Rietveld analysis. The characterized materials contained minor impurity $LaBO_3$, which was hardly to be removed although the various attempts were tried. The occurrence of minor impurity is observed commonly in luminescence materials research, which complicates the luminescence spectra and often hinders someone to properly understand the spectra of luminescence materials if the luminescence was not discerned properly.[14,15] The present work demonstrated that luminescence from the main phase and the minor impurity can be well-discerned through carefully comparing the luminescence of the $Ca_3La_{3(1-x)}Ce_{3x}(BO_3)_5$ mixture materials with that for $LaBO_3$:1%Ce^{3+} material, even though the luminescence of the

Received: March 22, 2012
Published: August 8, 2012

   dx.doi.org/10.1021/ic3006053 | Inorg. Chem. 2012, 51, 8802−8809

main phase arises from two distinct sites. The excitation spectra of $LaBO_3:Ce^{3+}$ in VUV−UV range are reported as well here for the first time.[16,17]

2. EXPERIMENTAL SECTION

A series of polycrystalline samples of $Ca_3La_3(BO_3)_5:xCe^{3+}$ were prepared by a solid-state reaction route at high temperature. The reactants include analytical reagent grade $CaCO_3$, H_3BO_3, and 99.99% pure rare-earth oxides CeO_2 and La_2O_3. According to the nominal compositions of compounds $Ca_3La_{3(1-x)}Ce_{3x}(BO_3)_5$ (x = 0, 0.01, 0.04, 0.10, 0.30, 0.50), the stoichiometric starting materials with 3 mol % excess of H_3BO_3 to compensate for the B_2O_3 volatilization were ground in an agate mortar and heated in air at 700 °C for 2 h. After the samples were slowly cooled down to room temperature, they were thoroughly reground and then calcined at 1100 °C for 10 h in CO reducing atmosphere, which was produced by the incomplete combustion of carbon powder during the high-temperature reaction. From phase analysis, a small amount of second phase of $LaBO_3$ was always found in $Ca_3La_3(BO_3)_5:xCe^{3+}$ samples, despite we did various attempts to remove it, such as adjusting temperature, sintering time, raw material ratio, and so on. In order to clarify the influence of the impurity phase $LaBO_3:Ce^{3+}$ on the spectra of $Ca_3La_3(BO_3)_5:Ce^{3+}$ samples, we have prepared $La_{0.99}Ce_{0.01}BO_3$ in a similar way for comparison with $Ca_3La_3(BO_3)_5:xCe^{3+}$ samples.

The phase purity of the samples was examined by X-ray diffraction (XRD) using a D8 ADVANCE powder diffractometer with Cu Kα radiation at room temperature. High-quality XRD data for Rietveld refinement were collected over a 2θ range from 8° to 100° at an interval of 0.02°. Structure refinements of XRD data were performed using Topas Academic software.[18]

The steady-state excitation and corresponding emission spectra in UV−vis range were measured with a FLS920 spectrometer equipped with a CTI-cryogenics temperature controlling system, and a 450 W xenon lamp was used as the excitation source. The decay curves were recorded on an Edinburgh FLSP920 spectrometer with excitation photons from a 150 W nF900 ns flash lamp with a pulse width of 1 ns and pulse repetition rate of 40−100 kHz. The vacuum ultraviolet (VUV) excitation and corresponding luminescence spectra were measured at the VUV spectroscopy experimental station on beamline 4B8 of Beijing Synchrotron Radiation Facility (BSRF). The measurement details have been described elsewhere.[19]

3. RESULTS AND DISCUSSION

3.1. XRD Refinement. The powder XRD patterns of $Ca_3La_{3(1-x)}Ce_{3x}(BO_3)_5$ (x = 0, 0.01, 0.04, 0.10, 0.30, and 0.50) compounds are shown in Figure 1, which are consistent with the reported pattern of $Ca_3La_3(BO_3)_5$ in JCPDS (31-0277). There are weak diffraction lines from the second-phase $LaBO_3$ (marked with asterisks ∗) in each diffractogram.

In order to confirm the structure and evaluate the content of impurity phase, Rietveld structure refinements for $Ca_3La_{3(1-x)}Ce_{3x}(BO_3)_5$ (x = 0, 0.01, 0.04, 0.10, 0.30, and 0.50) compounds were performed using the powder diffraction data. The $P6_3mc$ structure reported by Zhou et al.[13] was used as an initial model in the Rietveld analysis. The refined unit cell parameters and residual factors are summarized in Table 1. As shown in Table 1, with the increase of Ce^{3+} doping concentration, the a-axis and c-axis, as well as the unit cell volume, become slightly smaller, indicating that Ce^{3+} ions have been effectively dissolved into the $Ca_3La_3(BO_3)_5$ host lattice. Initially the occupancies of Ce^{3+} on La^{3+} and Ca^{2+} sites were refined with chemical composition constraint applied according to the nominal Ce^{3+} content, which suggests that the Ce^{3+} cations enter into both the La^{3+} and Ca^{2+} sites. This is consistent with the two-center luminescence of Ce^{3+}, which will be discussed in the later section. According to the composition

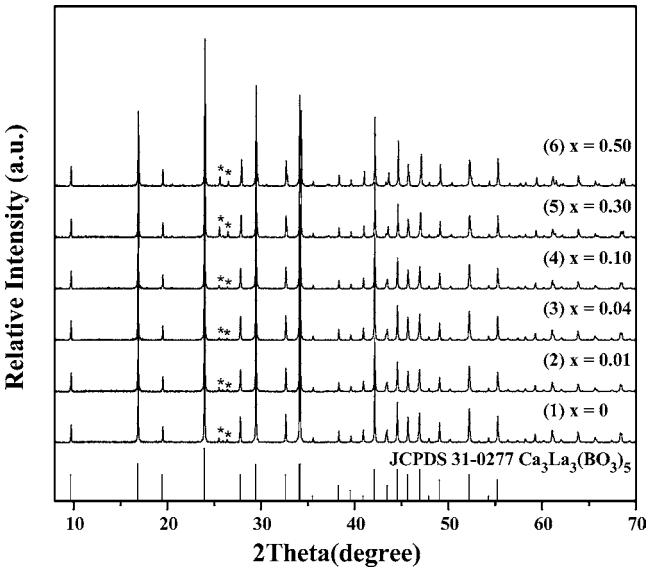

Figure 1. XRD patterns of $Ca_3La_{3(1-x)}Ce_{3x}(BO_3)_5$ (x = 0, 0.01, 0.04, 0.10, 0.30, and 0.50). The peaks marked by ∗ belong to the minor impurity phase $LaBO_3$.

of $Ca_3La_{3(1-x)}Ce_{3x}(BO_3)_5$, the occupation of Ce^{3+} on Ca^{2+} site requires partial Ca^{2+} ions entering into La^{3+} site to balance the charge. Thus the possible anti-site disorder between La^{3+}/Ce^{3+} and Ca^{2+} has to be considered. At the next stage of refinement, the occupancies of La^{3+}, Ca^{2+}, and Ce^{3+} ions on both the La^{3+} site and the Ca^{2+} site were refined with composition constraints applied according to their nominal values. In addition, the planar BO_3 geometry constraint was applied during the refinement. The final refined occupancies of $La^{3+}/Ce^{3+}/Ca^{2+}$ on the La^{3+} and Ca^{2+} sites are listed in Table 1. The minor impurities $LaBO_3$ in $Ca_3La_3(BO_3)_5:xCe^{3+}$ (x = 0, 0.01, 0.04, 0.10, 0.30, and 0.50) samples were refined, and the percentages of $LaBO_3$ from the two-phase Rietveld refinements are also listed in Table 1, showing that the percentage of the minor phase $LaBO_3$ is changed from 0.64 to 3.27 wt % in the $Ca_3La_{3(1-x)}Ce_x(BO_3)_5$ (x = 0−0.5) samples. Figure 2 shows the Rietveld fit of XRD pattern for $Ca_3La_{2.97}Ce_{0.03}(BO_3)_5$.

The incorporation of Ce^{3+} ions into both the La^{3+} and Ca^{2+} sites in $Ca_3La_{3(1-x)}Ce_{3x}(BO_3)_5$ samples is consistent with the fact that the cationic size of Ce^{3+} lies between those for Ca^{2+} and La^{3+}, that is, the radius (1.14 Å) of Ce^{3+} in 8-fold coordination is between those of Ca^{2+} (1.12 Å) and La^{3+} (1.16 Å), and the radius (1.25 Å) of Ce^{3+} in 10-fold coordination is between those of Ca^{2+} (1.23 Å) and La^{3+} (1.27 Å).[20] The refinement showed that La^{3+} ions have no occupation on the Ca^{2+} site on all of the Ce^{3+}-doped samples, consistent with the complete ordering of La^{3+} and Ca^{2+} observed in the undoped material $Ca_3La_3(BO_3)_5$. Therefore the observed antisite disorder in the Ce^{3+}-doped materials is confined between Ca^{2+} and Ce^{3+}; in other words, it is the Ce^{3+}-doping that introduces the antisite disorder in the Ce^{3+}-doped samples. The preferred location of Ce^{3+} ions on the La^{3+} site over the Ca^{2+} site (as shown in Table 1) is in agreement with the fact that Ce^{3+} is closer to La^{3+} than Ca^{2+} on the chemical bonding. Figure 3a shows the projection of the structure of $Ca_3La_3(BO_3)_5$ along the c-axis direction. The structure consists of a three-dimensional network made up of BO_3 triangles as well as irregular oxygen polyhedra of lanthanum and calcium atoms. La^{3+} ion has 10-fold coordination, while Ca^{2+} ion is

dx.doi.org/10.1021/ic3006053 | Inorg. Chem. 2012, 51, 8802−8809

Table 1. Crystallographic Data and Structure Parameters of $Ca_3La_3(BO_3)_5$:xCe^{3+}[a]

sample	CLBO	CLBO:0.01Ce^{3+}	CLBO:0.04Ce^{3+}	CLBO:0.10Ce^{3+}	CLBO:0.30Ce^{3+}	CLBO:0.50Ce^{3+}
cell parameters						
space group	$P6_3mc$ (hexagonal)					
a (Å)	10.5098(1)	10.5095(1)	10.5112(1)	10.5081(1)	10.5065(1)	10.5050(1)
c (Å)	6.41935(7)	6.41808(7)	6.41455(8)	6.41329(8)	6.40123(6)	6.38831(6)
V (Å^3)	614.05(1)	613.90(1)	613.76(1)	613.27(1)	611.94(1)	610.53 (1)
reliability factor						
R_{wp}(%)	3.73	3.46	3.78	3.80	3.78	3.86
R_p(%)	2.49	2.33	2.49	2.52	2.49	2.60
R_B(%)	0.78	0.66	1.13	1.36	0.88	1.07
occupancy of $La^{3+}/Ca^{2+}/Ce^{3+}$ on the La^{3+} site						
La	1	0.992(1)	0.959(1)	0.902(1)	0.702(1)	0.504(1)
Ce	0	0.008(2)	0.028(2)	0.072(1)	0.251(1)	0.426(1)
Ca	0	0.002(2)	0.013(1)	0.029(1)	0.051(1)	0.077(1)
occupancy of Ca^{2+}/Ce^{3+} on the Ca^{2+} site						
Ca	1	0.999(3)	0.990(2)	0.972 (2)	0.950(2)	0.919(2)
Ce	0	0.002(2)	0.013(1)	0.029(1)	0.051(1)	0.077(1)
weight percentage of $LaBO_3$	1.24	1.02	0.64	1.18	3.27	2.58

[a] CLBO:xCe^{3+}; x = 0, 0.01, 0.04, 0.10, 0.30, and 0.50.

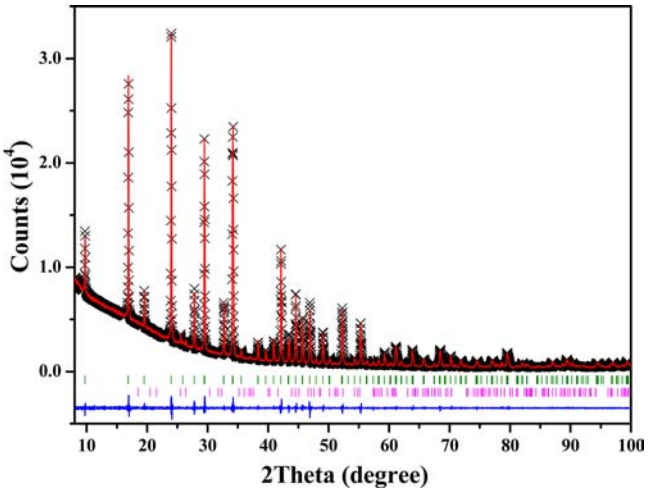

Figure 2. The experimental (crosses) and calculated (red solid line) XRD patterns and their difference (blue solid line) for $Ca_3La_{2.97}Ce_{0.03}(BO_3)_5$. The bottom row of Brag positions belongs to the second phase $LaBO_3$ with content of 1.02 wt %.

surrounded by eight oxygen atoms, as given in Figure 3b,c. The La−O and Ca−O interatomic distances in $Ca_3La_{2.97}Ce_{0.03}(BO_3)_5$ are listed in Table 2. The LaO_{10} polyhedron exhibits one short La−O distance 2.39(1) Å, and nine long La−O distances from 2.45(1) to 2.808(2) Å. The distances between Ca and O are in the range of 2.33(1)−2.57(2) Å. Both sites for La^{3+} and Ca^{2+} ions are in C_s symmetry.

3.2. Luminescence of Ce^{3+} in $LaBO_3$. Because about 0.64−3.27 wt % $LaBO_3$ impurities are found in $Ca_3La_3(BO_3)_5$:xCe^{3+} samples, luminescence of Ce^{3+} in the impurity may hinder us from correctly understanding the spectra of $Ca_3La_3(BO_3)_5$:Ce^{3+}. To exclude the influence of the luminescence of $LaBO_3$:Ce^{3+} on that of $Ca_3La_3(BO_3)_5$:Ce^{3+}, it is necessary to clearly discern the spectra of $LaBO_3$:Ce^{3+}. Therefore, we prepared and measured the luminescence of phosphor $La_{0.99}Ce_{0.01}BO_3$. In $LaBO_3$, La^{3+} occupies a 9-fold coordination site with C_s symmetry, and the average La−O

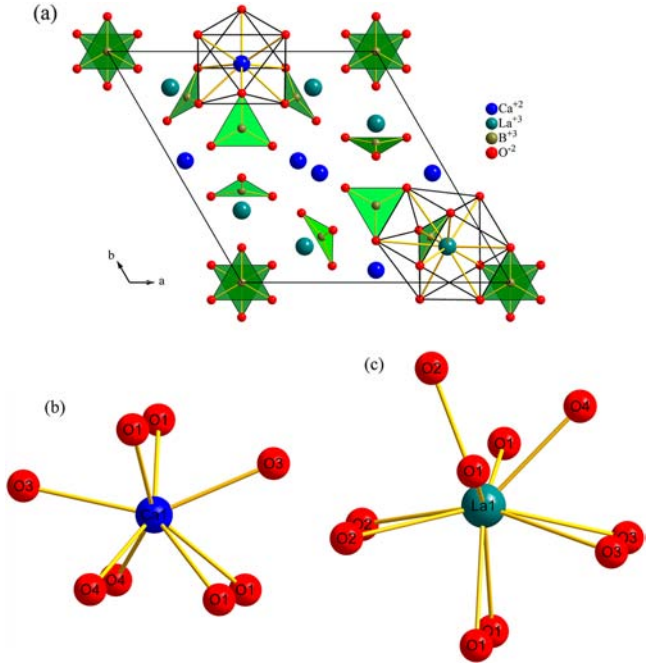

Figure 3. (a) Crystal structure of $Ca_3La_3(BO_3)_5$ along the c-axis direction. (b) Ca is 8-fold coordinated by 8 O; (c) La is 10-fold coordinated by 10 O.

Table 2. Interatomic Distances of Ca−O and La−O in $Ca_3La_{2.97}Ce_{0.03}(BO_3)_5$ Sample

atom1−atom2	interatomic distance (Å)	atom1−atom2	interatomic distance (Å)
La−O1(×2)	2.557(7)	Ca−O1(×2)	2.33(1)
La−O1(×2)	2.74(1)	Ca−O1(×2)	2.57(2)
La−O2(×2)	2.79(1)	Ca−O3	2.35(3)
La−O2	2.39(1)	Ca−O3	2.43(2)
La−O3(×2)	2.808(2)	Ca−O4(×2)	2.334(8)
La−O4	2.45(1)	avg (Ca−O)	2.406
avg (La−O)	2.663		

dx.doi.org/10.1021/ic3006053 | Inorg. Chem. 2012, 51, 8802−8809

bond distance is about 2.59 Å. Ce^{3+} ions should be incorporated into the La^{3+} sites in $La_{0.99}Ce_{0.01}BO_3$.

Figure 4a displays the area normalized emission spectra of $La_{0.99}Ce_{0.01}BO_3$ under 330, 266, 239, and 172 nm excitations at

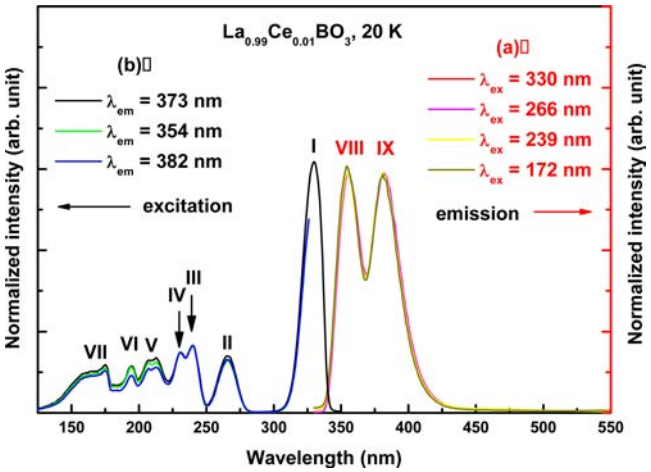

Figure 4. The excitation (λ_{em} = 373, 354, and 382 nm) and emission (λ_{ex} = 330, 266, 239, and 172 nm) spectra of $La_{0.99}Ce_{0.01}BO_3$ at 20 K.

20 K. These four excitation wavelengths correspond to bands I, II, and III and host-related absorption in Figure 4b. Four normalized emission spectra nearly overlapped one another, suggesting that bands I, II, and III may arise from Ce^{3+} in the same lattice site. Two broad bands, VIII (~355 nm) and IX (~381 nm), are observed in each curve, which should be the transitions from the relaxed lowest 5d to ^2F_J (J = 5/2, 7/2) states of Ce^{3+} in $LaBO_3$. Their positions are in good agreement with those reported in the literature.[21]

By monitoring the emissions at 373 nm, 354 nm (band VIII), and 382 nm (band IX), we recorded the VUV−UV excitation spectrum of $La_{0.99}Ce_{0.01}BO_3$ at 20 K (Figure 4b). After being normalized to the height of band III, these three emission spectra nearly overlapped with each other, reinforcing that Ce^{3+} ions just occupy one type of lattice site in $LaBO_3$. Seven broad bands, I (~330 nm), II (~266 nm), III (~240 nm), IV (~231 nm), V (~212 nm), VI (~195 nm), and VII (~175 nm), can be found in the spectrum. Band I is much stronger than the other bands. The excitation above wavelength 180 nm with a peak at about 175 nm (band VII) is due to host-related absorption, because many borates have host-related absorption in this spectral range.[22−24] Band VI may relate to the 4f−6s transition of Ce^{3+} in the host or other unknown sources. Bands I−V are due to 4f → 5d transitions of Ce^{3+} in $LaBO_3$. Hence, the centroid energy and the crystal field splitting of Ce^{3+} in $LaBO_3$ is estimated to be 40.0×10^3 and 16.9×10^3 cm^{-1}, respectively. To our knowledge, the detailed VUV−UV excitation spectrum of $LaBO_3$:Ce^{3+} has not been reported in any source, except for the Ph.D. thesis of Mayolet.[16,17] These values are in good agreement with those depicted before. The spectroscopic data of $LaBO_3$:Ce^{3+} are listed in Table 3.

3.3. Luminescence of Ce(1)$^{3+}$ Center in $Ca_3La_3(BO_3)_5$.

Figure 5 shows the excitation (a, λ_{em} = 390 nm; c, λ_{em} = 452 nm) and emission (b_1, λ_{ex} = 311 nm; b_2, λ_{ex} = 330 nm; d, λ_{ex} = 370 nm) spectra of $Ca_3La_{2.97}Ce_{0.03}(BO_3)_5$ measured at liquid helium temperature (LHT). In curve a, when we monitored the emission at 390 nm (band E), four excitation bands, I (~331

Table 3. The Spectroscopic Data of $LaBO_3$:Ce^{3+} and $Ca_3La_3(BO_3)_5$:Ce^{3+}

host	spectral origin	wavelength (nm)	symbol
$LaBO_3$	five 4f−5d excitation bands of Ce^{3+} (20 K)	330, 266, 240, 231, 212	I, II, III, IV, V
	emission of Ce^{3+} (20 K)	355, 381	VIII, IX
$Ca_3La_3(BO_3)_5$	five 4f−5d excitation bands of $Ce(1)^{3+}$ (20 K)	309, 269, 258, 246, 217	A, B, C, K, L
	emission of $Ce(1)^{3+}$ (LHT)	365, 390	D, E
	lowest 4f−5d excitation band of $Ce(2)^{3+}$ (LHT)	370	F
	emission of $Ce(2)^{3+}$ (LHT)	421, 455	G, J

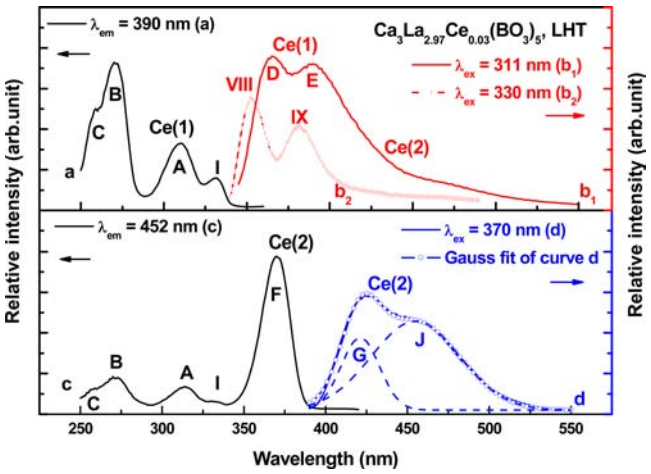

Figure 5. The excitation (a, λ_{em} = 390 nm; c, λ_{em} = 452 nm) and emission (b_1, λ_{ex} = 311 nm, b_2, λ_{ex} = 330 nm; d, λ_{ex} = 370 nm) spectra of $Ca_3La_{2.97}Ce_{0.03}(BO_3)_5$ at LHT. The peak deconvolution of Gaussian components (bands G and J) are shown for the emission spectrum d.

nm), A (~310 nm), B (~270 nm), and C (~259 nm), can be observed.

It is reasonable to think that band I corresponds to the lowest 4f−5d excitation band of Ce^{3+} in impurity $LaBO_3$, when the following three facts were considered. First, as shown in Table 1, there is 1.02 wt % $LaBO_3$ impurity in the sample $Ca_3La_{2.97}Ce_{0.03}(BO_3)_5$, and the position of band I in Figure 5 is almost the same as that in Figure 4. Second, because the emission of $LaBO_3$:Ce^{3+} covers the spectral range from ~340 to ~410 nm, when we monitored the emission at 390 nm, band I might be observed in Figure 5 although the content of $LaBO_3$ impurity is very low, because the intensity of band I is extremely strong (in Figure 4). Third, upon 330 nm (band I) excitation, the emission spectrum is displayed in curve b_2, which is clearly different from curve b_1 under 311 nm (band A) excitation. Two emission bands VIII (~352 nm) and IX (~382 nm) can be read in this emission spectrum. The positions of bands VIII and IX and the spectral shape are nearly the same with those in Figure 4 ($LaBO_3$:Ce^{3+}).

The other three bands, A, B, and C, are the 4f → 5d excitation bands of Ce^{3+} in $Ca_3La_3(BO_3)_5$. The band A should be the lowest 4f → 5d excitation band. Because the refinement suggests that Ce^{3+} can enter two distinct sites (Ca^{2+} and La^{3+} sites) in $Ca_3La_3(BO_3)_5$; here, we denote the band A is the lowest 4f → 5d excitation band of $Ce(1)^{3+}$ center in $Ca_3La_3(BO_3)_5$ for the time being. Its nature will be assigned later. As shown in curve d of Figure 5, because emission of the $Ce(2)^{3+}$ center is very weak at our monitoring emission

dx.doi.org/10.1021/ic3006053 | Inorg. Chem. 2012, 51, 8802−8809

wavelength 390 nm, all these three bands A, B, and C may belong to the excitation bands of the $Ce(1)^{3+}$ center.

Upon 311 nm (band A) excitation, the emission spectrum was recorded in curve b_1 (Figure 5). Two bands, D (~365 nm) and E (~390 nm), were detected in the spectrum. Because the absorption of impurity $LaBO_3:Ce^{3+}$ is very low at about 310 nm, as shown in Figure 4b, and the energy transfer (ET) between two phases is often of low efficiency, it is reasonable to exclude the influence of impurity $LaBO_3:Ce^{3+}$ on this emission spectrum. Consequently, bands D and E are marked as 5d → 4f emissions of the $Ce(1)^{3+}$ center in $Ca_3La_3(BO_3)_5$. Stokes shift of the $Ce(1)^{3+}$ center is evaluated to be about 4.1×10^3 cm^{-1}. The tail band at the long-wavelength side of the $Ce(1)^{3+}$ emission is from $Ce(2)^{3+}$ center due to $Ce(1)^{3+} \rightarrow Ce(2)^{3+}$ energy transfer.

Curve c in Figure 5 is the excitation spectrum by monitoring the emission at 452 nm (band J). A very strong band F (~370 nm), two obvious bands A and B, and two weak bands C and I can be observed. Bands A, B, C, and I have been depicted before. Clearly, band F is the lowest 4f → 5d excitation band of $Ce(2)^{3+}$ in $Ca_3La_3(BO_3)_5$. Because of effective spectral overlapping between the excitation band F of the $Ce(2)^{3+}$ center and the emission bands D and E of the $Ce(1)^{3+}$ center, it is predictable that energy transfer from $Ce(1)^{3+}$ to $Ce(2)^{3+}$ occurred, as shown in Figure 5.

Upon 370 nm (band F) excitation, the emission spectrum was measured and shown in curve d (Figure 5). A broad band peaking at about 420 nm was observed, which has a shoulder band at the long-wavelength side. The emission would be just from the $Ce(2)^{3+}$ center in $Ca_3La_3(BO_3)_5$. To estimate the band positions of $Ce(2)^{3+}$ doublet emissions, we fitted this emission curve with a sum of two Gaussian profiles with maxima at about 421 nm (band G) and 455 nm (band J), respectively. Accordingly, Stokes shift of the $Ce(2)^{3+}$ center is estimated to be about 3.3×10^3 cm^{-1}.

To ascertain all possible positions of $Ce(1)^{3+}$ 4f → 5d excitation bands, we measured the VUV−UV excitation spectra of $Ca_3La_{2.97}Ce_{0.03}(BO_3)_5$ at 20 K by monitoring the emission at 389 nm (band E) and 357 nm (near band VIII), respectively. Figure 6 shows the normalized emission spectra. Seven excitation bands can be seen in each spectrum, as indicated in Figure S1 in the Supporting Information. The band H with a maximum at about 176 nm can be attributed to host-related absorption.[10,22−24] Below the wavelength of ~290 nm, two normalized spectra are almost overlapping each other. The relative intensity of band A and band I shows some differences in the two curves. When the monitoring wavelength shifts from 389 to 357 nm, the intensity of band I increases, while that of band A decreases. As observed in curves b_1 and b_2 of Figure 5, this is because the emission intensity of $Ca_3La_{2.97}Ce_{0.03}(BO_3)_5$ decreases from 389 to 357 nm but that of $LaBO_3:Ce^{3+}$ increases. Therefore, it is reasonable to assume that band I belongs to the 5d excitation band of Ce^{3+} in impurity $LaBO_3$ and bands L, K, C, B, and A are mainly from 4f → 5d excitation of the $Ce(1)^{3+}$ center in $Ca_3La_{2.97}Ce_{0.03}(BO_3)_5$.

Figure 7 shows the emission spectra of $Ca_3La_{2.97}Ce_{0.03}(BO_3)_5$ with minor impurity $LaBO_3:Ce^{3+}$ (a, λ_{ex} = 172 nm; b, λ_{ex} = 221 nm; c, λ_{ex} = 269 nm; d, λ_{ex} = 309 nm) at 20 K. Under 172 nm excitation, a very broad band with a maximum at about 360 nm was observed in curve a. This band is asymmetric with a tail at the long-wavelength side. The peak of this band has a large difference from those in curves b, c, and d. Based on the discussion before, the emission of $LaBO_3:Ce^{3+}$ may have great contribution to curve a, so the peak moves to the short-wavelength side with respect to other three curves. The weak tail band may belongs to the emission of $Ca_3La_{2.97}Ce_{0.03}(BO_3)_5$. Because the content of impurity is very low in the sample, this observation seems to suggest that the energy transfer from host to Ce^{3+} center in $LaBO_3$ is significantly higher than that in $Ca_3La_3(BO_3)_5$.

Since the wavelength 221 nm is close to the peak L and the wavelength 269 nm corresponds to the peak B in Figure 6, it is predictable that the emission from $Ce(1)^{3+}$ center should be dominant under 221 and 269 nm excitation, respectively. This is indeed observed in curves b and c. On the other hand, we cannot exclude the emission of $LaBO_3:Ce^{3+}$ impurity in curves b and c due to the existence of 4f−5d excitation bands around these two excitation wavelengths. Meanwhile, because of the energy transfer of $Ce(1)^{3+} \rightarrow Ce(2)^{3+}$, the emission from the

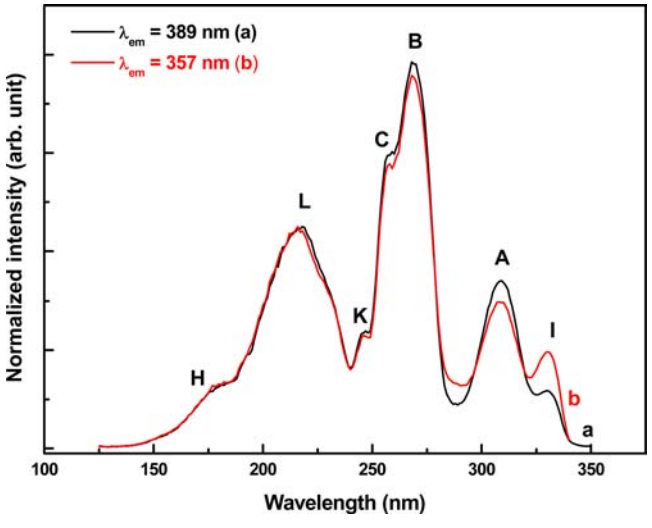

Figure 6. The VUV−UV excitation spectra of $Ca_3La_{2.97}Ce_{0.03}(BO_3)_5$ (a, λ_{em} = 389 nm; b, λ_{em} = 357 nm) at 20 K.

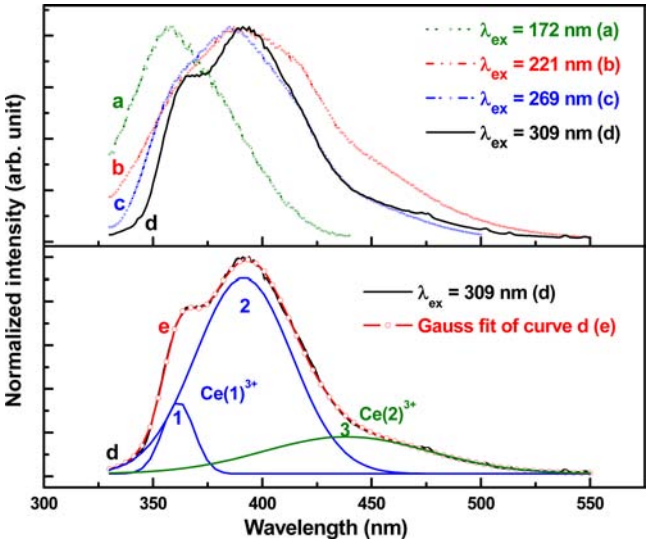

Figure 7. The emission spectra of $Ca_3La_{2.97}Ce_{0.03}(BO_3)_5$ with minor impurity $LaBO_3:Ce^{3+}$ (a, λ_{ex} = 172 nm; b, λ_{ex} = 221 nm; c, λ_{ex} = 269 nm; d, λ_{ex} = 309 nm) at 20 K. The peak deconvolution of Gaussian components 1−3 are shown for the emission spectrum d.

dx.doi.org/10.1021/ic3006053 | Inorg. Chem. 2012, 51, 8802−8809

$Ce(2)^{3+}$ center also occurs in curves b and c. Furthermore, it is interesting to point out that the $Ce(2)^{3+}$ emission intensity in curve b is evidently stronger than that in curve c. This phenomenon seems to suggest that $Ce(2)^{3+}$ center has a 5d excitation band around 221 nm. This factor together with the $Ce(1)^{3+} \rightarrow Ce(2)^{3+}$ energy transfer result in the stronger $Ce(2)^{3+}$ emission under 221 nm excitation.

In the last case, when samples were excited at 309 nm, the lowest 5d excitation band of $Ce(1)^{3+}$ center, we recorded the emission spectrum in curve d of Figure 7, which is like curve b_1 in Figure 5 and can be well-fitted with a sum of three Gaussian functions (curve e in Figure 7). Three Gaussian bands have maxima at about 361, 391, and 438 nm, respectively, which are in good agreement with those in Figure 5.

From Figure 7, it can be found that the emission intensity of $Ce(1)^{3+}$ is always stronger than that of $Ce(2)^{3+}$ regardless of the excitation wavelength. According to the Rietveld structural refinement, about 80% of Ce^{3+} ions are expected to enter La^{3+} site and about 20% of Ce^{3+} ions are likely to occupy Ca^{2+} site for the sample $Ca_3La_{3(1-x)}Ce_{3x}(BO_3)_5$ (x = 0.01, see Table 1). Taking into account the low-doping concentration of Ce^{3+} in this sample, it is reasonable to ignore the concentration-quenching of both sites. As a consequence, the $Ce(1)^{3+}$ center should be the 10-fold coordination La^{3+} site with C_s symmetry. Then, another Ce^{3+} center, the $Ce(2)^{3+}$ center, should be the 8-fold coordination Ca^{2+} site with C_s symmetry.

3.4. Luminescence of $Ce(2)^{3+}$ Center in $Ca_3La_3(BO_3)_5$. A concentrated sample, $Ca_3La_{3(1-x)}Ce_{3x}(BO_3)_5$ (x = 0.10), was selected to investigate the 5d excitation bands of $Ce(2)^{3+}$ sites, because most Ce^{3+} ions occupy La^{3+} sites [i.e., $Ce(1)^{3+}$ sites, ~80%] in diluted sample $Ca_3La_{3(1-x)}Ce_{3x}(BO_3)_5$ (x = 0.01). Figure 8 shows the excitation spectra of $Ca_3La_{3(1-x)}Ce_{3x}(BO_3)_5$ (x = 0.10) in VUV–UV–vis range.

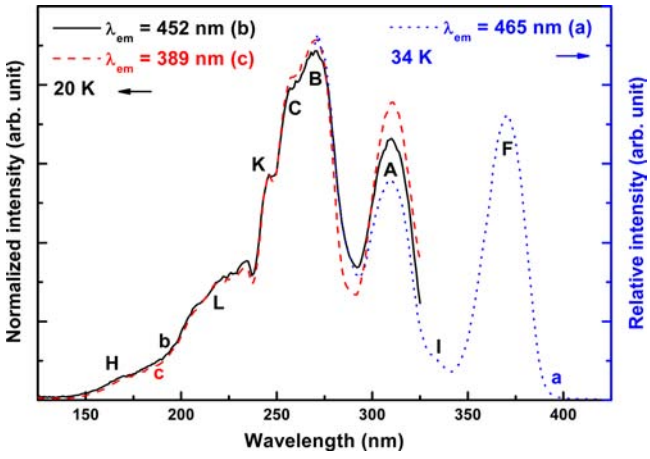

Figure 8. Excitation spectra of $Ca_3La_{3(1-x)}Ce_{3x}(BO_3)_5$ (x = 0.10; a, λ_{em} = 465 nm, 34 K; b, λ_{em} = 452 nm, 20 K; c, λ_{em} = 389 nm, 20 K) in VUV–UV–vis range.

The lowest 5d excitation band F of $Ce(2)^{3+}$ centers is detected in curve a. In curves b and c, the two monitoring emission wavelengths, 389 and 452 nm, are near the peak E of the $Ce(1)^{3+}$ center and the peak J of the $Ce(2)^{3+}$ center in Figure 5, respectively. Two normalized excitation spectra are unchanged whenever we monitored the emission from the $Ce(1)^{3+}$ center or that from the $Ce(2)^{3+}$ center, showing that the emission wavelength has no influence on the excitation. Though the spectral shape shows some differences from Figure 6, the bands A, B, C, K, and L, as summarized in Table 3, were observed in each curve as well. Hence, the spectra a and b still can be considered to mainly consist of excitation bands of the $Ce(1)^{3+}$ center.

This observation is also in line with the structural data, see Table 1. It is estimated that about 29% of Ce^{3+} ions enter Ca^{2+} sites for this high-doping sample, $Ca_3La_{3(1-x)}Ce_{3x}(BO_3)_5$ (x = 0.10), by Rietveld structural refinement. Though the occupation probability of the $Ce(2)^{3+}$ relative to the $Ce(1)^{3+}$ in $Ca_3La_{3(1-x)}Ce_{3x}(BO_3)_5$ (x = 0.10) is higher than that in low-doping sample $Ca_3La_{3(1-x)}Ce_{3x}(BO_3)_5$ (x = 0.01), the occupancy of the $Ce(1)^{3+}$ center is still dominant. So other 5d excitation bands of $Ce(2)^{3+}$ cannot be measured except for the lowest one. To our knowledge, the technique of time-resolved spectroscopy may be helpful to solve this problem,[25] but we cannot perform this measurement at present due to the limitation of experimental conditions at BSRF.

3.5. Influence of Doping Concentration on Luminescence of Ce^{3+}. To evaluate the influence of doping concentration (x value) on the emission intensity of Ce^{3+} ions in two sites, we normalized all emission spectra upon excitation of the $Ce(1)^{3+}$ center at 311 nm in the wavelength range 340–550 nm in Figure 9a. The emission from $Ce(2)^{3+}$

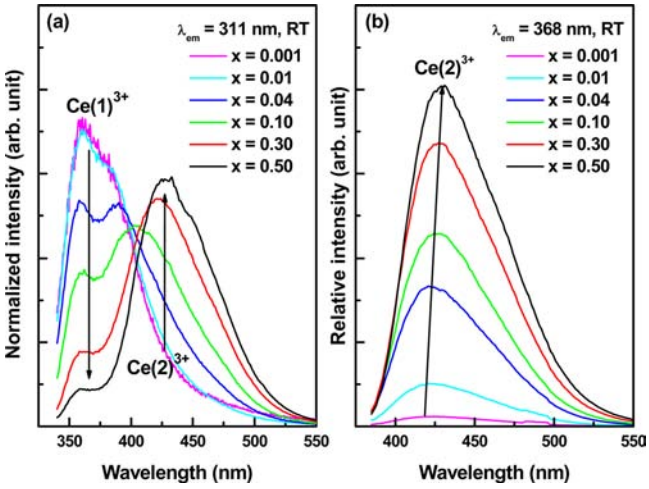

Figure 9. The emission spectra of samples $Ca_3La_{3(1-x)}Ce_{3x}(BO_3)_5$ with different x values at RT: (a) the normalized emission (λ_{ex} = 311 nm); (b) the emission spectra (λ_{ex} = 368 nm).

gradually increases with the increase of the x value, whereas the emission from $Ce(1)^{3+}$ decreases regularly. Meanwhile, emission intensity from $Ce(2)^{3+}$ always keeps increasing when excitation is on the $Ce(2)^{3+}$ center at 368 nm (Figure 9b). This may be due to two main factors: one is the different occupancy probability between $Ce(1)^{3+}$ and $Ce(2)^{3+}$; the other is the energy transfer from the $Ce(1)^{3+}$ center to the $Ce(2)^{3+}$ center.

First, Rietveld refinements have shown that the occupancy probability of the $Ce(1)^{3+}$ in the La^{3+} site is always higher than that of the $Ce(2)^{3+}$ in the Ca^{2+} site, and the occupations of both the $Ce(1)^{3+}$ and $Ce(2)^{3+}$ increase with the total doping concentration. So the emission from either the $Ce(1)^{3+}$ center or the $Ce(2)^{3+}$ center will regularly increase before the occurrence of concentration-quenching. Second, the lowest 5d absorption band F for the $Ce(2)^{3+}$ center was observed at about 370 nm, which has obvious overlap with the emission bands D and E from the $Ce(1)^{3+}$ center in Figure 5. This

dx.doi.org/10.1021/ic3006053 | Inorg. Chem. 2012, 51, 8802–8809

spectroscopic superposition will result in the $Ce(2)^{3+}$ ions absorbing the emission from the $Ce(1)^{3+}$ center efficiently. As a consequence, an effective resonance-type energy transfer may occur from $Ce(1)^{3+}$ to $Ce(2)^{3+}$, and this energy transfer will quench the emission of $Ce(1)^{3+}$ and weaken its emission intensity. The higher the doping concentration is, the higher is the probability that the energy transfer occurs. Accordingly the emission intensity from $Ce(1)^{3+}$ is expected to become weaker and weaker. These two reasons make the emission from the $Ce(2)^{3+}$ center increase but that from the $Ce(1)^{3+}$ center decrease.

In addition, it is interesting to note that the emission of the $Ce(2)^{3+}$ center slightly shifts to the long-wavelength side with the increase of Ce^{3+} doping concentration, as shown in Figure 9b, though the ionic radius of 8-fold coordination Ca^{2+} (~112 pm) is slightly smaller than that of Ce^{3+} (~114 pm).[20] The main reason for this phenomenon is that the lattice parameters reduce with the doping concentration, as shown in Rietveld refinement results, which could be explained by the radius of Ce^{3+} being slightly smaller than that of La^{3+} [$r(Ce^{3+})$ = 125 pm, $r(La^{3+})$ = 127 pm, 10-fold coordination], and most Ce^{3+} ions are incorporated into the La^{3+} sites. In consequence, the strength of crystal field around both Ce^{3+} centers increases gradually, which makes the lowest 5d state lower and results in the emission shifting to the long-wavelength side.

3.6. Luminescence Decay Characteristics. The decay curves were measured for all $Ca_3La_{3(1-x)}Ce_{3x}(BO_3)_5$ samples with various x as displayed in Figure 10. Upon excitation of band F at 368 nm and monitoring emission at 452 nm of band J, we obtained the luminescence decay curves of the $Ce(2)^{3+}$ center as shown in Figure 10a. These curves can be well fitted using a single exponential equation, $I_t = I_0 \exp(-t/\tau)$, where I_t and I_0 are the luminescence intensities, t is the time, and τ is the decay time. The value of τ around 36.5 ns is hardly influenced by the doping concentration. This observation is consistent with the results mentioned above that concentration quenching of the $Ce(2)^{3+}$ luminescence is not of much significance in the investigated concentration range.

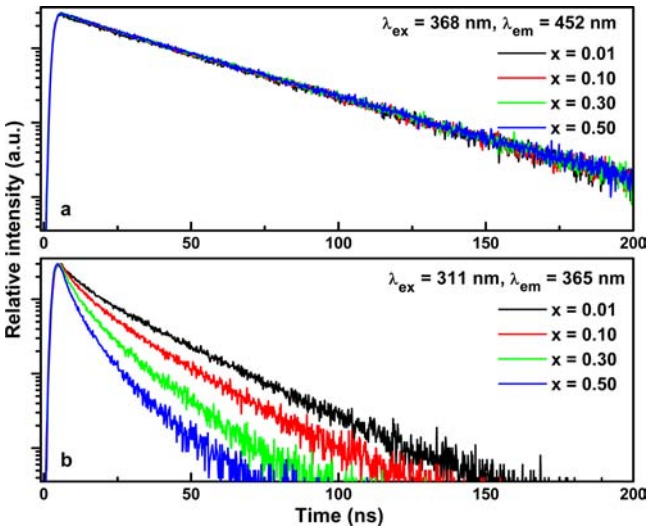

Figure 10. The decay curves of samples $Ca_3La_{3(1-x)}Ce_{3x}(BO_3)_5$ (x = 0.01, 0.10, 0.30, and 0.50) at RT.

Under excitation of band A at 311 nm and monitoring the emission of band D at 365 nm, we obtained the luminescence decay spectra of the $Ce(1)^{3+}$ center, as shown in Figure 10b. With the increase of the doping concentration, the decay time of the $Ce(1)^{3+}$ center clearly shortens. This confirms that the energy transfer rate from $Ce(1)^{3+}$ to $Ce(2)^{3+}$ increases with the Ce^{3+} doping concentration.

4. CONCLUSION

Phosphors $Ca_3La_3(BO_3)_5$:xCe^{3+} were prepared by a solid state reaction route at high temperature. The Rietveld refinement results showed that about 0.64−3.27 wt % $LaBO_3$ impurities exist in the $Ca_3La_3(BO_3)_5$:xCe^{3+} samples. The spectroscopic properties of $LaBO_3$:0.01Ce^{3+} displayed that the emission bands from $LaBO_3$:0.01Ce^{3+} are at about 355 and 381 nm, and the lowest 5d absorption band at 330 nm for Ce^{3+} in $LaBO_3$ is much stronger than other 5d bands. As a result, the lowest 5d absorption band for Ce^{3+} in $LaBO_3$ appeared in the excitation spectra of $Ca_3La_3(BO_3)_5$:Ce^{3+} when the monitoring wavelength is in the range of 330−450 nm. The investigations on the steady state excitation and emission spectra in the VUV−vis range together with Rietveld refinement results revealed that Ce^{3+} ions occupy two distinct sites in the $Ca_3La_3(BO_3)_5$ host lattice. The lowest 5d absorption band for the $Ce(1)^{3+}$ center has a maximum at about 310 nm, and that for the $Ce(2)^{3+}$ center at about 370 nm. The emission bands from the $Ce(1)^{3+}$ center are around 365 and 390 nm, while those from the $Ce(2)^{3+}$ center are around 421 and 455 nm. In terms of the structure of the host lattice, the $Ce(1)^{3+}$ center is assigned to the La^{3+} site, and the $Ce(2)^{3+}$ center to the Ca^{2+} site. Because the distribution of Ce^{3+} over the available sites changes with concentration, and there exists energy transfer from the $Ce(1)^{3+}$ center to the $Ce(2)^{3+}$ center; the luminescence from the $Ce(2)^{3+}$ center increases at the expense of that from the $Ce(1)^{3+}$ center with the increase of Ce^{3+} concentration. The decay characteristics of Ce^{3+} in two centers confirmed the existence of the energy transfer from the $Ce(1)^{3+}$ center to the $Ce(2)^{3+}$ center.

■ ASSOCIATED CONTENT

Supporting Information

The crystal structure of $Ca_3La_{3(1-x)}Ce_{3x}(BO_3)_5$ (x = 0, 0.01, 0.04, 0.10, 0.30, and 0.50) in CIF format, and the peak convolution of Gaussian components of the VUV−UV excitation spectra of $Ca_3La_{2.97}Ce_{0.03}(BO_3)_5$ monitored at 389 nm. This material is available free of charge via the Internet at http://pubs.acs.org.

■ AUTHOR INFORMATION

Corresponding Author

*E-mail: cesbin@mail.sysu.edu.cn.

Notes

The authors declare no competing financial interest.

■ ACKNOWLEDGMENTS

The work is financially supported by the National Natural Science Foundation of China (Grant Nos. 10979027 and 21171176).

■ REFERENCES

(1) Shimizu, Y.; Sakano. K.; Noguchi,Y.; Moriguchi, T. U.S. Patent No. 5998925, 1998.

(2) Huang, C. H.; Chen, T. M. *J. Phys. Chem. C* **2011**, *115*, 2349−2355.

(3) Wang, X. M.; Wang, C. H.; Wu, M. M.; Wang, Y. X.; Jing, X. P. *J. Mater. Chem.* **2012**, *22*, 3388−3394.
(4) Holloway, P. H.; Trottier, T. A.; Abrams, B.; Kondoleon, C.; Jones, S. L.; Sebastian, J. S.; Thomas, W. J.; Swart, H. *J. Vac. Sci. Technol. B* **1999**, *17*, 758−764.
(5) Blasse, G.; Grabmaier, B. C. *Luminescent Materials*; Springer-Verlag: Berlin, Germany, 1994.
(6) Wang, L.; Zhang, X.; Hao, Z. D.; Luo, Y. S.; Zhang, L. G.; Zhong, R. X.; Zhang, J. H. *J. Electrochem. Soc.* **2012**, *159*, F68−F72.
(7) Dorenbos, P. *J. Lumin.* **2000**, *91*, 155−176.
(8) Lin, H. H.; Liang, H. B.; Han, B.; Zhong, J. P.; Su, Q. *Phys. Rev. B* **2007**, *76*, No. 035117.
(9) Shionoga, S.; Yen, W. M. *Phosphor Handbook*; CRC: Boston, MA, 1999.
(10) Han, B.; Liang, H. B.; Lin, H. H.; Zhong, J. P.; Su, Q.; Zhang, G. B.; Fu, Y. B. *Appl. Phys. A: Mater. Sci. Process.* **2007**, *88*, 705−709.
(11) Zhang, Y.; Li, Y. D.; Yin, Y. S. *J. Alloys Compd.* **2005**, *400*, 222−226.
(12) Zhang, Y.; Liang, J. K.; Chen, X. L.; He, M.; Xu., T. *J. Alloys Compd.* **2001**, *327*, 96−99.
(13) Zhou, T. Y.; Ye, N. *Acta Crystallogr., Sect. E: Struct. Rep. Online* **2008**, *64*, I37−U105.
(14) Peng, Y. A.; Guo, F. Y. *Spectrosc. Spectral Anal.* **1994**, *14*, 15−20.
(15) Guo, F. Y.; Chang, S. L. *J. Rare Earth* **1990**, *8*, 229−232.
(16) Dorenbos, P. *Phys. Rev. B* **2001**, *64*, No. 125117.
(17) Mayolet, A. Ph.D. thesis, Universite de Paris XI Orasy, France, 1995.
(18) Coelho, A. A. TOPAS ACADEMIC, version 4, Brisbane, Australia, 2005.
(19) Tao, Y.; Huang, Y.; Gao, Z. H.; Zhuang, H.; Zhou, A. Y.; Tan, Y. L.; Li, D. W.; Sun, S. S. *J. Synchrotron Radiat.* **2009**, *16*, 857−863.
(20) Shannon, R. D. *Acta Crystallogr.* **1976**, *A32*, 751−767.
(21) Blasse, G.; Bril, A. *J. Chem. Phys.* **1967**, *47*, 5139−5145.
(22) Liang, H. B.; Su, Q; Tao, Y.; Xu, J. H.; Huang, Y. *Mater. Res. Bull.* **2006**, *41*, 1468−1475.
(23) Kwon, I. E.; Yu, B. Y.; Bae, H.; Hwang, Y. J.; Kwon, T. W.; Kim, C. H.; Pyun, C. H.; Kim, S. J. *J. Lumin.* **2000**, *87*−*89*, 1039−1041.
(24) Jüstel, T.; Krupa, J. C.; Wiechert, D. U. *J. Lumin.* **2001**, *93*, 179−189.
(25) Omelkov, S. I.; Brik, M. G.; Kirm, M.; Pustovarov, V. A.; Kiisk, V.; Sildos, I.; Lange, S; Lobanov, S. I.; Isaenko, L. I. *J. Phys.: Condens. Matter* **2011**, *23*, No. 105501.